arXiv:2308.01238v1 [astro-ph.HE] 2 Aug 2023

IXPE and XMM-Newton observations of the Soft Gamma Repeater SGR 1806−20

Roberto Turolla,[1,2] Roberto Taverna,[1] Gian Luca Israel,[3] Fabio Muleri,[4] Silvia Zane,[2] Matteo Bachetti,[5] Jeremy Heyl,[6] Alessandro Di Marco,[4] Ephraim Gau,[7] Henric Krawczynski,[7] Mason Ng,[8] Andrea Possenti,[5] Juri Poutanen,[9] Luca Baldini,[10,11] Giorgio Matt,[12] Michela Negro,[13,14,15] Iván Agudo,[16] Lucio A. Antonelli,[17,18] Wayne H. Baumgartner,[19] Ronaldo Bellazzini,[10] Stefano Bianchi,[20] Stephen D. Bongiorno,[19] Raffaella Bonino,[21,22] Alessandro Brez,[10] Niccolò Bucciantini,[23,24,25] Fiamma Capitanio,[4] Simone Castellano,[10] Elisabetta Cavazzuti,[26] Chieng-Ting Chen,[27,19] Stefano Ciprini,[17,28] Enrico Costa,[4] Alessandra De Rosa,[4] Ettore Del Monte,[4] Laura Di Gesu,[26] Niccolò Di Lalla,[29] Immacolata Donnarumma,[26] Victor Doroshenko,[30] Michal Dovčiak,[31] Steven R. Ehlert,[19] Teruaki Enoto,[32] Yuri Evangelista,[4] Sergio Fabiani,[4] Riccardo Ferrazzoli,[4] Javier A. Garcia,[33] Shuichi Gunji,[34] Kiyoshi Hayashida,[35,*] Wataru Iwakiri,[36] Svetlana G. Jorstad,[37,38] Philip Kaaret,[39,19] Vladimir Karas,[31] Fabian Kislat,[40] Takao Kitaguchi,[32] Jeffery J. Kolodziejczak,[19] Fabio La Monaca,[4] Luca Latronico,[22] Ioannis Liodakis,[41] Simone Maldera,[22] Alberto Manfreda,[10] Frédéric Marin,[42] Andrea Marinucci,[26] Alan P. Marscher,[37] Herman L. Marshall,[8] Francesco Massaro,[43,22] Ikuyuki Mitsuishi,[44] Tsunefumi Mizuno,[45] C.-Y. Ng,[46] Stephen L. O'Dell,[19] Nicola Omodei,[29] Chiara Oppedisano,[22] Alessandro Papitto,[18] George G. Pavlov,[47] Abel L. Peirson,[29] Matteo Perri,[17,18] Melissa Pesce-Rollins,[10] Pierre-Olivier Petrucci,[48] Maura Pilia,[5] Simonetta Puccetti,[17] Brian D. Ramsey,[19] John Rankin,[4] Ajay Ratheesh,[4] Oliver J. Roberts,[27,19] Roger W. Romani,[29] Carmelo Sgró,[10] Patrick Slane,[49] Paolo Soffitta,[4] Gloria Spandre,[10] Douglas A. Swartz,[27,19] Toru Tamagawa,[32,50,51] Fabrizio Tavecchio,[52] Yuzuru Tawara,[44] Allyn F. Tennant,[19] Nicholas E. Thomas,[19] Francesco Tombesi,[53,28,54] Alessio Trois,[5] Sergey S. Tsygankov,[9] Jacco Vink,[55] Martin C. Weisskopf,[19] Kinwah Wu,[2] and Fei Xie[4,56]

[1] *Dipartimento di Fisica e Astronomia, Università degli Studi di Padova, Via Marzolo 8, I-35131 Padova, Italy*
[2] *Mullard Space Science Laboratory, University College London, Holmbury St Mary, Dorking, Surrey RH5 6NT, UK*
[3] *INAF Osservatorio Astronomico di Roma, via Frascati 33, I-00078 Monteporzio Catone, Italy*
[4] *INAF Istituto di Astrofisica e Planetologia Spaziali, Via del Fosso del Cavaliere 100, I-00133 Roma, Italy*
[5] *INAF Osservatorio Astronomico di Cagliari, Via della Scienza 5, I-09047 Selargius (CA), Italy*
[6] *Department of Physics and Astronomy, University of British Columbia, Vancouver, BC V6T 1Z1, Canada*
[7] *Physics Department and McDonnell Center for the Space Sciences, Washington University in St. Louis, St. Louis, MO 63130, USA*
[8] *MIT Kavli Institute for Astrophysics and Space Research, Massachusetts Institute of Technology, 77 Massachusetts Avenue, Cambridge, MA 02139, USA*
[9] *Department of Physics and Astronomy, FI-20014 University of Turku, Finland*
[10] *Istituto Nazionale di Fisica Nucleare, Sezione di Pisa, Largo B. Pontecorvo 3, I-56127 Pisa, Italy*
[11] *Dipartimento di Fisica, Università di Pisa, Largo B. Pontecorvo 3, I-56127 Pisa, Italy*
[12] *Dipartimento di Matematica e Fisica, Università degli Studi Roma Tre, Via della Vasca Navale 84, I-00146 Roma, Italy*
[13] *University of Maryland, Baltimore County, Baltimore, MD 21250, USA*
[14] *NASA Goddard Space Flight Center, Greenbelt, MD 20771, USA*
[15] *Center for Research and Exploration in Space Science and Technology, NASA/GSFC, Greenbelt, MD 20771, USA*
[16] *Instituto de Astrofísica de Andalucía-CSIC, Glorieta de la Astronomía s/n, E-18008, Granada, Spain*
[17] *Space Science Data Center, Agenzia Spaziale Italiana, Via del Politecnico snc, I-00133 Roma, Italy*
[18] *INAF Osservatorio Astronomico di Roma, Via Frascati 33, I-00078 Monte Porzio Catone (RM), Italy*
[19] *NASA Marshall Space Flight Center, Huntsville, AL 35812, USA*
[20] *Dipartimento di Matematica e Fisica, Università degli Studi Roma Tre, Via della Vasca Navale 84, I-00146 Roma, Italy*
[21] *Dipartimento di Fisica, Università degli Studi di Torino, Via Pietro Giuria 1, I-10125 Torino, Italy*
[22] *Istituto Nazionale di Fisica Nucleare, Sezione di Torino, Via Pietro Giuria 1, I-10125 Torino, Italy*
[23] *INAF Osservatorio Astrofisico di Arcetri, Largo Enrico Fermi 5, I-50125 Firenze, Italy*
[24] *Dipartimento di Fisica e Astronomia, Università degli Studi di Firenze, Via Sansone 1, I-50019 Sesto Fiorentino (FI), Italy*
[25] *Istituto Nazionale di Fisica Nucleare, Sezione di Firenze, Via Sansone 1, I-50019 Sesto Fiorentino (FI), Italy*
[26] *Agenzia Spaziale Italiana, Via del Politecnico snc, I-00133 Roma, Italy*
[27] *Universities Space Research Association (USRA)*
[28] *Istituto Nazionale di Fisica Nucleare, Sezione di Roma Tor Vergata, Via della Ricerca Scientifica 1, I-00133 Roma, Italy*

Corresponding author: Roberto Turolla
turolla@pd.infn.it

[29] Department of Physics and Kavli Institute for Particle Astrophysics and Cosmology, Stanford University, Stanford, CA 94305, USA

[30] Institut für Astronomie und Astrophysik, Universität Tübingen, Sand 1, D-72076 Tübingen, Germany

[31] Astronomical Institute of the Czech Academy of Sciences, Boční II 1401/1, 14100 Praha 4, Czech Republic

[32] RIKEN Cluster for Pioneering Research, 2-1 Hirosawa, Wako, Saitama 351-0198, Japan

[33] California Institute of Technology, Pasadena, CA 91125, USA

[34] Yamagata University, 1-4-12 Kojirakawa-machi, Yamagata-shi 990-8560, Japan

[35] Osaka University, 1-1 Yamadaoka, Suita, Osaka 565-0871, Japan

[36] International Center for Hadron Astrophysics, Chiba University, Chiba 263-8522, Japan

[37] Institute for Astrophysical Research, Boston University, 725 Commonwealth Avenue, Boston, MA 02215, USA

[38] Department of Astrophysics, St. Petersburg State University, Universitetsky pr. 28, Petrodvoretz, 198504 St. Petersburg, Russia

[39] University of Iowa Department of Physics and Astronomy, Van Allen Hall, 30 N. Dubuque Street, Iowa City, IA 52242, USA

[40] University of New Hampshire Department of Physics & Astronomy Space Science Center Morse Hall, Rm 311 8 College Rd Durham, NH 03824

[41] Finnish Centre for Astronomy with ESO, FI-20014 University of Turku, Finland

[42] Université de Strasbourg, CNRS, Observatoire Astronomique de Strasbourg, UMR 7550, F-67000 Strasbourg, France

[43] Dipartimento di Fisica, Università degli Studi di Torino, Via Pietro Giuria 1, I-10125 Torino, Italy

[44] Graduate School of Science, Division of Particle and Astrophysical Science, Nagoya University, Furo-cho, Chikusa-ku, Nagoya, Aichi 464-8602, Japan

[45] Hiroshima Astrophysical Science Center, Hiroshima University, 1-3-1 Kagamiyama, Higashi-Hiroshima, Hiroshima 739-8526, Japan

[46] Department of Physics, The University of Hong Kong, Pokfulam, Hong Kong

[47] Department of Astronomy and Astrophysics, Pennsylvania State University, University Park, PA 16802, USA

[48] Université Grenoble Alpes, CNRS, IPAG, F-38000 Grenoble, France

[49] Center for Astrophysics, Harvard & Smithsonian, 60 Garden Street, Cambridge, MA 02138, USA

[50] RIKEN Nishina Center, 2-1 Hirosawa, Wako, Saitama 351-0198, Japan

[51] Department of Physics, Tokyo University of Science, 1-3 Kagurazaka, Shinjuku, Tokyo 162-8601, Japan

[52] INAF Osservatorio Astronomico di Brera, Via E. Bianchi 46, I-23807 Merate (LC), Italy

[53] Dipartimento di Fisica, Università degli Studi di Roma Tor Vergata, Via della Ricerca Scientifica 1, I-00133 Roma, Italy

[54] Department of Astronomy, University of Maryland, College Park, MD 20742, USA

[55] Anton Pannekoek Institute for Astronomy & GRAPPA, University of Amsterdam, Science Park 904, 1098 XH Amsterdam, The Netherlands

[56] Guangxi Key Laboratory for Relativistic Astrophysics, School of Physical Science and Technology, Guangxi University, Nanning 530004, People's Republic of China

ABSTRACT

Recent observations with the Imaging X-ray Polarimetry Explorer (IXPE) of two anomalous X-ray pulsars provided evidence that X-ray emission from magnetar sources is strongly polarized. Here we report on the joint IXPE and XMM-Newton observations of the soft γ-repeater SGR 1806–20. The spectral and timing properties of SGR 1806–20 derived from XMM-Newton data are in broad agreement with previous measurements; however, we found the source at an all-time-low persistent flux level. No significant polarization was measured apart from the 4–5 keV energy range, where a probable detection with PD = $31.6 \pm 10.5\%$ and PA = $-17°.6^{+15°.5}_{-15°.0}$ was obtained. The resulting polarization signal, together with the upper limits we derive at lower and higher energies (2–4 and 5–8 keV, respectively) is compatible with a picture in which thermal radiation from the condensed star surface is reprocessed by resonant Compton scattering in the magnetosphere, similar to what proposed for the bright magnetar 4U 0142+61.

Keywords: X-rays: stars — stars: magnetars — techniques: polarimetric

1. INTRODUCTION

Soft γ-repeaters (SGRs) and anomalous X-ray pulsars (AXPs) form together a small class of Galactic X-ray

* Deceased

pulsars, characterized by long spin periods ($P \sim$ 1–12 s), high spin-down rates $\dot{P} \sim 10^{-15}$–10^{-10} s s^{-1} and the emission of short, energetic bursts of hard X-/soft gamma-rays. The huge inferred values of the (spin-down) dipole field ($B \sim 10^{13}$–10^{15} G), the lack of a detected binary companion and a persistent X-ray lu-

minosity, $L_{\rm X} \sim 10^{30}$–$10^{35}\,{\rm erg\,s^{-1}}$, typically in excess of the spin-down power, indicate that these sources are magnetars, ultra-magnetized neutron stars powered by their own magnetic energy (Duncan & Thompson 1992; Thompson & Duncan 1993, see also Turolla et al. 2015; Kaspi & Beloborodov 2017 for reviews and Olausen & Kaspi 2014 for a catalogue of magnetar sources[1]).

Because of the super-strong magnetic fields they host, the opacities of the two normal polarization modes are way different so the X-ray emission from SGRs/AXPs is expected to be highly polarized (up to $\approx 80\%$; Fernández & Davis 2011; Taverna et al. 2014, 2020; Caiazzo et al. 2022). Theoretical predictions were finally tested when the NASA-ASI Imaging X-ray Polarimetry Explorer (IXPE; Weisskopf et al. 2022), the first satellite designed to provide imaging polarimetry in the 2–8 keV band, observed the two brightest magnetar sources, the AXPs 4U 0142+61 and 1RXS J170849.0–400910 (hereafter 1RXS J1708 for short) during the first year of operations. Polarization was clearly detected in the 2–8 keV band at the $\approx 13.5\%$ level in the former and to a much higher degree, $\approx 35\%$, in the latter (Taverna et al. 2022; Zane et al. 2023).

In both sources the polarization strongly depends on energy. In 1RXS J1708 it monotonically increases from $\approx 20\%$ up to $\approx 80\%$ at constant polarization angle, possibly indicating that 2–8 keV photons come from regions of the star surface with different properties: a magnetic condensate (either solid or liquid) and an atmosphere (Zane et al. 2023). On the other hand, in 4U 0142+61 it first decreases from $\approx 15\%$ to zero at around 4–5 keV where the polarization angle swings by $90°$, and then rises to $\approx 35\%$, suggesting that thermal radiation from a condensed surface patch is then reprocessed by resonant Compton scattering (RCS; Thompson et al. 2002; Fernández & Thompson 2007; Nobili et al. 2008) onto mildly relativistic electrons flowing in the star's twisted magnetosphere (Taverna et al. 2022, an alternative interpretation in terms of mode switching in a magnetized atmosphere was recently put forward by Lai 2023).

Polarization measurements in strongly magnetized neutron stars can probe vacuum birefringence, a strong-field, quantum electrodynamics (QED) effect predicted more than 80 years ago but never experimentally tested as yet (see e.g. Heyl & Shaviv 2000, 2002, and references therein). Although previous magnetar observations are in agreement with QED predictions, no smoking-gun evidence for vacuum birefringence was found, mostly

[1] Available online at
http://www.physics.mcgill.ca/~pulsar/magnetar/main.html

because thermal emission in both 4U 0142+61 and 1RXS J1708 comes from a fairly limited area of the star surface, so its intrinsic polarization is preserved at infinity anyway, even if no vacuum birefringence is present (see van Adelsberg & Perna 2009; Santangelo et al. 2019).

Further magnetar observations with IXPE are required to address this issue and also to provide fresh insight into the similarities/differences among magnetar sources. Here we report on the simultaneous IXPE and XMM-Newton observations of the prototypical magnetar SGR 1806–20. The XMM-Newton and IXPE observations are detailed in §2 and the results of the timing, spectral and polarimetric analyses are presented in §3. Discussion follows in §4.

2. OBSERVATIONS

First identified as a high-energy transient in the KONUS data over 40 years ago (Mazets et al. 1981), SGR 1806–20 was shortly after realized to be a repeater (Atteia et al. 1987; Kouveliotou et al. 1987; Laros et al. 1987). The source, located at about 8.7 kpc from the Sun (Bibby et al. 2008), is a regular and prolific emitter of short bursts clustered in active periods, one of which occurred in 2004 and culminated on 2004 December 27 with the emission of the most powerful giant flare (GF) observed so far from a magnetar ($L \approx 10^{47}\,{\rm erg\,s^{-1}}$; Hurley et al. 2005; Palmer et al. 2005).

SGR 1806–20 spins with a period $P \approx 7.5\,{\rm s}$; the period derivative increased from $\dot{P} = 8 \times 10^{-11}\,{\rm s\,s^{-1}}$ to $5 \times 10^{-10}\,{\rm s\,s^{-1}}$ in 2000–2011 and then went back to the "historical" value (see Younes et al. 2017). The latter implies a surface (dipole) field of $B = 8 \times 10^{14}\,{\rm G}$, the highest ever recorded. The steady X-ray emission in the 0.5–10 keV range, $L_{\rm X} \approx 10^{35}\,{\rm erg\,s^{-1}}$ (for the assumed distance of 8.7 kpc), is well described by the superposition of a blackbody (BB) and a power law (PL) component, with (slightly variable) temperature $kT \approx 0.6\,{\rm keV}$, blackbody radius ≈ 1–$2\,{\rm km}$ and spectral index $\Gamma \approx 1.6$ (Mereghetti et al. 2005b; Woods et al. 2007; Younes et al. 2015, 2017). The power law tail extends, seemingly unbroken, into higher energies (up to ≈ 200 keV; see, e.g., Mereghetti et al. 2005a; Younes et al. 2017). The pulse profile is double-peaked with a pulsed fraction PF ≈ 3–8% in a wide energy range (Woods et al. 2007; Younes et al. 2015, 2017).

The emission of a bright burst detected by several instruments on 2023, February 23 (Brivio et al. 2023; Mereghetti et al. 2023) marked the onset of a renewed period of activity from SGR 1806–20. To catch the source in an active state, IXPE observed SGR 1806–20

starting on 2023, March 22. In addition a DDT pointing with XMM-Newton was activated.

2.1. XMM-Newton

SGR 1806–20 was observed with the European Photon Imaging Camera (EPIC) on board the XMM-Newton satellite starting on 2023-04-07 00:18:48 UTC for an exposure time of about 45 ks. The EPIC-pn (Strüder et al. 2001) was operating in Full Frame mode (FF; timing resolution of 73.4 ms). The MOS cameras (Turner et al. 2001) were set in Small Window mode (SW; timing resolution of 0.3 s).

Standard procedures were applied in the extraction of the scientific products. Time intervals of high background activity were removed, resulting in a net exposure of 34.9 ks and 40.5 ks for the pn and the MOSs, respectively. We collected the source photons from within a circle of radius 42″. The background level was estimated from a circular region of radius 100″ centered far from the source, on the same CCD for the pn and, due to the reduced window, in a different CCD for the MOSs. We checked for the potential impact of pile-up with the EPATPLOT tool and found a negligible pile-up fraction of $\approx 0.4\%$. The response matrices and ancillary files were generated by means of the RMFGEN and ARFGEN tasks, respectively. The final source spectra were obtained by using SPECGROUP, rebinning the channels by a factor of three in order to match the intrinsic EPIC spectral resolution and imposing a minimum of 25 counts in each channel. Background-subtracted and exposure-corrected light curves were extracted using EPICLCCORR. The EPIC photon arrival times were referenced to the Solar System barycenter. The source was found at a count rate of $0.354(3)\,\mathrm{cts\,s^{-1}}$ (here and in the following uncertainties are reported at 1σ confidence level, unless specified otherwise).

2.2. IXPE

IXPE observed SGR 1806–20 from 2023-03-22 05:57:51 UTC to 2023-04-01 18:56:26 UTC and from 2023-04-03 11:41:03 UTC to 2023-04-13 22:20:20 UTC, for a total on-source time of ≈ 947 ks. Processed Level 2 (LV2) photon lists, one for each of the three IXPE detector units (DUs), were downloaded from the archive at HEASARC[2] and further processed to reduce the background with respect to the source signal.

Source and background counts were extracted from a circular region centered on the source position (identified with the brightest pixel in the IXPE image) with radius 36″ and from a concentric annulus with inner and outer

radius of 78″ and 240″, respectively. In order to discriminate the background events due to charged particles and high-energy photons without affecting the genuine X-ray events, we then applied the rejection criteria described in Di Marco et al. (2023). The counting rate as a function of time is shown in Figure 1. Time periods during which the background was larger than 50% of the source average counting rate are flagged and removed from the subsequent analysis. This step removes ≈ 6 out of the total ≈ 947 ks of the IXPE observation. Arrival times were corrected to the Solar System barycenter with the FTOOL BARYCORR included in HEASOFT 6.31.1, using the Jet Propulsion Laboratory Development Ephemeris 421 and the International Celestial Reference System frame.

3. RESULTS

3.1. XMM-Newton *Timing and Spectral analysis*

Both pn and MOS photon arrival time lists were used in order to look for the pulsar spin signal. We started from the timing properties inferred from the most recent spin measurements of SGR 1806–20 in 2015–2016 (Younes et al. 2017) and extrapolated them to the epoch of the new XMM-Newton dataset. In particular, we assumed a spin period $P = 7.7501(2)$ s and a first period derivative $\dot{P} = 7.5(2) \times 10^{-11}\,\mathrm{s\,s^{-1}}$, both referred to MJD 57202. The linear evolution of the period in 2015–2016 (see Figure 3 of Younes et al. 2017) and the relatively quiet behaviour of the source in the last few years, suggest that $\dot{P}$ is constant (or at most slightly variable) since then. Correspondingly, we analyzed the new XMM-Newton datasets searching for significant peaks in the 7.7659–7.7712 s period range, i.e. accounting for changes in P and $\dot{P}$ up to about 6σ with respect to the values reported by Younes et al. (2017).

Only one significant peak with a chance probability of about 9.6σ of not being a statistical fluctuation, and after having corrected for the number (530) of independent sampling periods of the search, was found in the Rayleigh periodogram. The period is 7.770 s. The modulation is present both in the pn and in the MOS data alone, confirming that the signal is intrinsic to the source and not an instrumental artefact. In order to obtain a more refined measurement we applied a phase-fitting technique, which resulted in a period of $7.7703(2)$ s (frequency $\nu = 0.128695(4)$ Hz); we derived also a 3σ upper limit on the period derivative, $|\dot{P}| < 2 \times 10^{-7}\,\mathrm{s\,s^{-1}}$. The 1–12 keV pulse shape is double-peaked, in agreement with the profiles obtained for SGR 1806–20 in the past (Younes et al. 2015). The pulsed fraction (defined as the semi-amplitude of the sinusoid divided by the
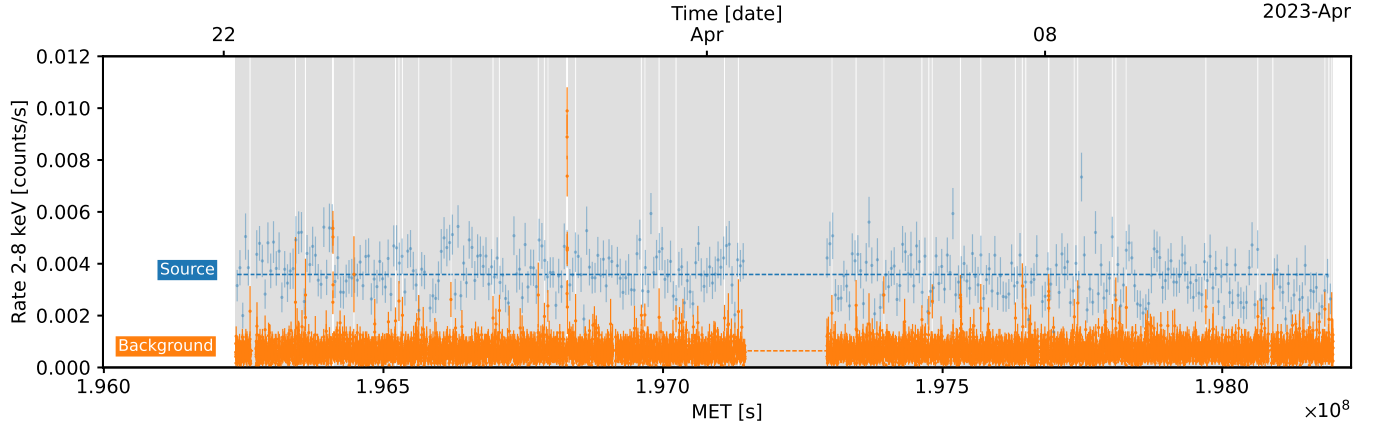
Figure 1. Count rate in the 2–8 keV energy range, summed over the three IXPE DUs, as a function of time for two regions in the field of view, one containing the source and the other only background. Periods in which the background was larger than 50% of the average source rate are identified by vertical white lines and removed by subsequent analyses. The time bin is 5000 s and 100 s for the source and background, respectively.

source average count rate) is PF = 5(1)% (see left panel of Figure 2).

The spectral analysis of SGR 1806–20 was performed by fitting simultaneously all the EPIC datasets within XSPEC (Arnaud 1996). A single component (absorbed) model, such as a PL or a BB, resulted in a poor fit (reduced $\chi^2 \approx 1.3$–3.1 for 300 dof). A BB+PL and a BB+BB model, often adopted to describe the 0.1–12 keV magnetar spectra, yield a good agreement with the data (reduced $\chi^2 \approx 1.17$ in both cases). The best-fitting parameters are listed in Table 1 and the EPIC spectra together with the best-fitting BB+PL model are shown in the right panel of Figure 2. We find that the addition of a second spectral component is significant to more than 6σ. Although the BB+BB and BB+PL models are equally acceptable on a statistical basis, in the following we refer to the latter. The BB+PL spectral decomposition has been widely adopted in the past for SGR 1806–20, and this choice is motivated by the clear detection of a power law tail e.g. in NuSTAR data (Younes et al. 2015, 2017). The inferred parameters are in agreement with the average values obtained in the past ten years, though the flux was unexpectedly a factor of about three lower than the average.

3.2. IXPE *timing and spectro-polarimetric analysis*

After background and solar-flare removal (see §2.2), no significant changes in both the source and background counts were detected in the two IXPE pointings, so that we used the combined data in our analysis.

We searched for pulsations using the Z_2^2 statistics (Buccheri et al. 1983), which is adequate for double-peaked pulsed profiles. We joined the event lists from the three DUs and ran the search using the quasi-fast folding algorithm described in Bachetti et al.

(2020, 2021). We searched over spin frequencies between 0.125 and 0.129 Hz, that contained the XMM-Newton solution, and frequency derivatives $|\dot{\nu}_{\rm spin}| < 4 \times 10^{-12}$ Hz s^{-1}. Given the low number of source counts (see below), we did not find significant peaks in the search; we derived a 5.2% pulsed fraction upper limit on pulsations over the frequency interval indicated above ($Z_2^2 \approx 25$; 90% c.l., evaluated following Vaughan et al. 1994). This upper limit is compatible with the detection with XMM-Newton of a $\approx 5\%$ pulsed fraction.

We extracted the Stokes parameters I, Q and U with the `xpbin` tool, exploiting the weighted analysis method (Di Marco et al. 2022) implemented in the latest version (30.3) of the IXPEOBSSIM software (Baldini et al. 2022)[3]. As a consequence of the limited number of counts (≈ 8000 background-subtracted events in the three DUs), the phase- and energy-integrated (2–8 keV) polarization degree, PD=$\sqrt{Q^2 + U^2}/I$, is 5.7%, below the MDP$_{99}$ (Weisskopf et al. 2010), which is about 20% for this observation and is therefore not significant[4]. The polarization angle, PA= $\arctan{(U/Q)}/2$, is then unconstrained. The same conclusion is reached by applying an analysis as outlined by Strohmayer (2017) within XSPEC, which provides PD $\approx 4.7\%$.

In order to test if a detectable polarization is present in some specific energy intervals, we performed an energy-resolved, phase-integrated (weighted) analysis in XSPEC. We started by dividing the IXPE working en-

---

[3] https://github.com/lucabaldini/ixpeobssim

[4] The minimum detectable polarization (MDP) is the largest signal expected to be produced by statistical fluctuations only, at a given confidence level (usually 99%, MDP$_{99}$). The result of a polarization measurement is regarded as significant if it exceeds MDP$_{99}$.
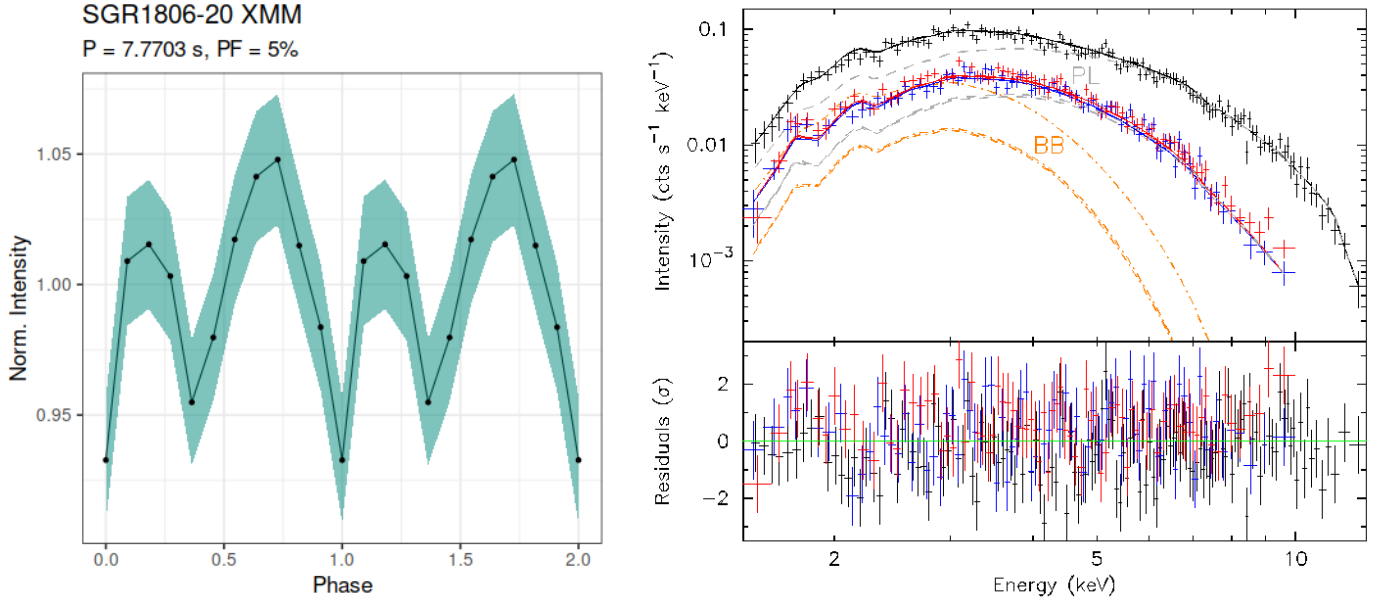
Figure 2. Left: The joint XMM-Newton 1-12 keV EPIC pn and MOS light curve folded to the best period inferred from the phase-fitting analysis (see text for details). The colored area marks the 1σ uncertainties on the data points. Right: EPIC-pn (black crosses/lines), MOS1 (blue crosses/lines) and MOS2 (red crosses/lines) spectra of SGR 1806–20 (upper panel), together with the fitting residuals, in units of standard deviation (lower panel), for the BB+PL model discussed in the text. The individual BB and PL components are shown by an orange dash-dotted and gray dashed line, respectively.

Table 1. Results of the XMM-Newton spectral fits.

Model	$N_{\rm H}$ $(10^{22}\,{\rm cm}^{-2})$	$kT_{\rm BB_1}$ (keV)	$R_{\rm BB_1}$[a] (km)	$\Gamma \mid kT_{\rm BB_2}$ $- \mid$ (keV)	Norm PL[b] $\mid R_{\rm BB_2}$[a] $- \mid$ (km)	Flux[c] (Obs $\mid$ Unabs) $(10^{-12}\,{\rm erg\,cm}^{-2}{\rm s}^{-1})$	χ^2/dof.
BB+PL	6.5±0.3	0.59±0.04	$1.3^{+0.3}_{-0.2}$	1.7 ± 0.1	$(1.3\pm0.3)\times10^{-3}$	4.3±0.1 $\mid$ 11.3 ± 0.4	351.9/298
BB+BB	5.7±0.2	0.70±0.03	1.2±0.1	2.4 ± 0.1	0.11±0.01	4.3±0.1 $\mid$ 8.2 ± 0.2	351.2/298

[a] Derived by adopting a 8.7 kpc distance (Bibby et al. 2008).

[b] In units of $\rm counts\,keV^{-1}\,cm^{-2}\,s^{-1}$.

[c] The fluxes are estimated in the 0.5–10 keV energy range.

ergy band into 6 equal bins (each 1-keV wide). The null hypothesis probability that the source is unpolarized in all the energy bins is $\approx 22\%$.

We found a signal with PD = $31.6 \pm 10.5\%$ (slightly higher than the MDP$_{99}$) and PA = $-17^\circ.6^{+15^\circ.5}_{-15^\circ.0}$, computed East of North, in the 4–5 keV range. No significant polarization was detected in the remaining bins. In particular, we found only an upper limit of 23% and 45% (99% confidence level) in the two neighbouring bins, 3–4 and 5–6 keV, respectively. Despite no firm conclusion can be reached about the trend of PD with energy, this may suggest that it increases in going from 3 to 4–5 keV. What happens at higher energies is harder to tell, essentially because the lower S/N ratio makes the MDP$_{99}$

higher and this translates into a weaker constraint on PD.

In order to improve the counting statistics we merged together the first and last pair of bins and considered the intervals 2–4, 4–5 and 5–8 keV. This did not produce any improvement, resulting again in an upper limit for PD of 24% and of 55% (99% confidence level) at low and high energies, respectively. Figure 3 shows the contour plots of the polarization degree and angle in each energy band, obtained with the XSPEC `steppar` command by assuming the spectral model obtained from the XMM-Newton observation. A somewhat different choice for the boundaries of the central interval, e.g. taking the bin

from 3.5 to 5 keV or from 4 to 5.5 keV, yields consistent results.

We also attempted a phase-dependent analysis by folding the data at the spin period derived from the XMM-Newton timing and assuming $\dot{P} = 7.5 \times 10^{-11}\,\mathrm{s\,s^{-1}}$ (see §3.1). No significant polarization was detected after dividing the pulse cycle the into 7 equally-spaced phase bins. In the next step we restricted to two phase bins, corresponding to the intervals [0.0, 0.38] and [0.38, 1.0], selected in such a way as to contain the secondary and primary peak of the pulse, respectively. Again no polarization was measured, either considering the entire 2–8 keV band or restricting to low (2–4 keV) and high (4–8 keV) energies. A negative result was also found limiting the analysis to the 4–5 keV range, where a phase-integrated signal was detected at 99% confidence level. This was expected given that the detection is marginal even when all the counts are considered.

An unbinned analysis (without background subtraction; González-Caniulef et al. 2023) in the 2–8 keV range shows that, when marginalized over the various parameters, the median polarization degree is ≈ 8.4% and about 1σ above zero. This is somewhat less than the MDP$_{99}$ of 10% for the observation without binning in phase or energy.

Fits to IXPE count spectra are rather inconclusive. Single component models, either an (absorbed) BB or PL, provide a (formally) acceptable agreement with the data. However, the BB fit yields a column density of $2.7 \times 10^{22}\,\mathrm{cm^{-2}}$, more than twice lower than that measured by XMM-Newton and previously reported in the literature. On the other hand, the parameters derived from the PL fit are consistent (within ≈ 1σ) with those from the XMM-Newton BB+PL fit, but this just reflects the limited IXPE energy range (2–8 keV). When a single PL model is extended to the entire XMM-Newton energy band the fit is no longer satisfactory (see §3.1). A fit with a two component model (BB+BB or BB+PL) leaving all the parameters free to vary is largely unconstrained, although by freezing all the parameters (except the normalizations) to those derived from the XMM-Newton data provides a good fit ($\chi^2 = 129.8$ for 162 dof).

A joint fit of the three Stokes parameters with the XSPEC model phabs× (bbodyrad×polconst +powerlaw×polconst), freezing again all the spectral parameters to those of the XMM-Newton analysis, does not provide any conclusive result. The upper limit (3σ confidence level) on the polarization degree of the PL is about 57% while the polarization of the BB is unconstrained. A similar conclusion is reached by truncating the PL at low energies. We remark that, while the fit is statistically acceptable in all these cases, nothing can be said about the relative polarization direction between the two components.

4. DISCUSSION

IXPE observed SGR 1806–20 in two segments for a total exposure time of about 1 Ms in March–April 2023. During the second stint, XMM-Newton targeted the source for about 45 ks to provide complementary spectral and timing information. Despite the renewed bursting activity, SGR 1806–20 was found at a (unabsorbed) flux level of $1.1 \times 10^{-11}\,\mathrm{erg\,cm^{-2}\,s^{-1}}$ in the 0.5–10 keV band, the lowest ever recorded, although still compatible within the uncertainties with the NuSTAR one reported by Younes et al. (2017). XMM-Newton spectra are well fitted by an (absorbed) BB+PL model and the spectral parameters ($kT_{\mathrm{BB}} = 0.6\,\mathrm{keV}$, $R_{\mathrm{BB}} = 1.3\,\mathrm{km}$, $\Gamma = 1.7$) are in broad agreement with those found by Younes et al. (2017). There is, however, a hint for a decrease of the BB radius with respect to the values measured by Younes et al. (2017) in 2015–2016, even if their NuSTAR data did not allow for a precise determination of the BB flux, and of a steepening of the PL with respect to the values measured by XMM-Newton in the same energy range prior to 2011 (Younes et al. 2015). The period and the upper limit for $\dot{P}$ we found are consistent with the past timing history of the source. The XMM-Newton pulse profile is double peaked with a pulsed fraction $PF \approx 5\%$, in agreement with previous measurements, while no pulsations were detected in the IXPE data.

The low flux level of SGR 1806–20 and the high background prevented a complete spectro-polarimentric and timing analysis of IXPE data. No pulsations were detected, with an upper limit of 5.2% on the pulsed fraction. Although poorly constrained, the IXPE spectrum is compatible with the BB+PL decomposition obtained from the analysis of XMM-Newton data. No significant polarization has been detected integrating over the source rotational period and in the 2–8 keV energy band.

Interestingly, by restricting the analysis to the 4–5 keV range we found a polarization signal significant at 99% confidence level, with PD ≈ 32% and PA ≈ −18°. At lower (2–4 keV) and higher (5–8 keV) energies only upper limits can be derived on PD, with values at 3σ of 24% and 55%, respectively.

Although XMM-Newton spectra are compatible with both a BB+PL and a BB+BB decomposition, the former is in our opinion favored, as discussed in §3.1. If the power law tail is associated with RCS, the predicted polarization degree saturates at 33% in the energy interval where this component dominates (Taverna et al.
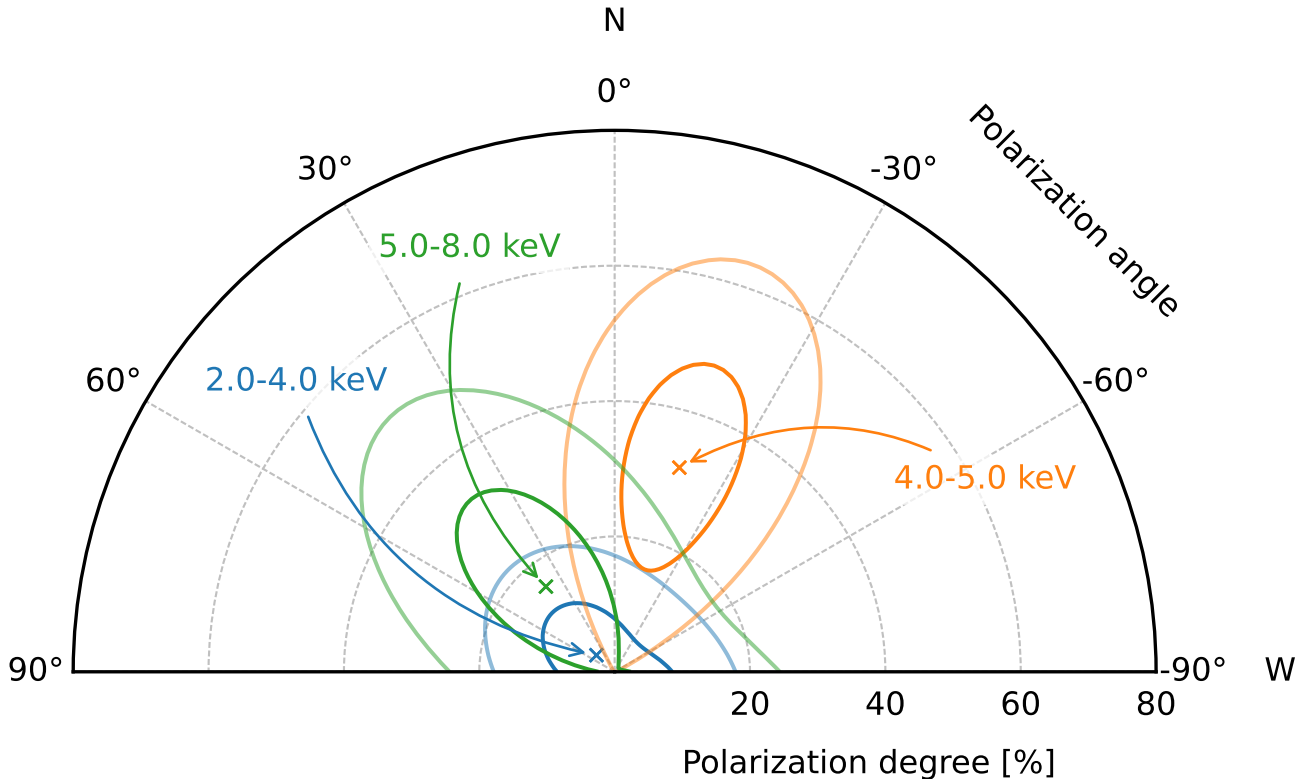
Figure 3. Contour plot of the IXPE polarization degree and angle in different energy bands. The inner and outer contours mark the regions at 68.3% and 99% confidence level, respectively. The spectral model is frozen to that obtained from the XMM-Newton observation.

2020). The thermal emission can originate either from a magnetized, cooling atmosphere, with PD ≈ 70–80% (except for very peculiar viewing geometries, see e.g. Taverna et al. 2015), or from the bare, condensed surface of the star, in which case a much lower PD ≲ 15–20% is expected. It has been also proposed that radiation emerging from atmospheres heated from above by particle bombardment has a modest polarization degree (comparable to that of the condensed surface, González-Caniulef et al. 2019; Doroshenko et al. 2022).

The constraints placed by the upper limits at low and high energies, together with a 99%-c.l. polarization degree of ≈ 32% at intermediate energies (where the thermal and non-thermal component coexist, see above) are compatible with a picture in which thermal emission comes from the bare NS surface or from an atmosphere heated by backflowing particles. This scenario was also applied to 4U 0142+61, where a clear 90° swing of PA with energy was detected, signalling that radiation is dominated by O-mode photons (coming from the condensed surface/heated atmosphere) at low energies and by X-mode photons (reprocessed by scatterings) at higher ones. The two sources may therefore be similar. Due to the low signal-to-noise ratio, no conclusion can

be drawn about the dependence of the polarization direction on the energy and hence on which polarization mode is prevailing in a given energy range. However, emission from a condensed surface/heated atmosphere can be either mostly in the X- or in the O-mode (depending e.g. on the orientation of the local magnetic field and the photon energy for the former and on the temperature gradient for the latter, see Taverna et al. 2022; Zane et al. 2023), so that a swing in PA is not necessarily expected.

Along this line, we explored a simple RCS model, in which thermal emission comes from two hot spots placed near the magnetic equator of the bare NS surface, including vacuum birefringence. With this choice of the emission geometry (similar to that adopted for 4U 0142+61), radiation from the magnetic condensate exhibits a relatively large polarization degree (≈ 20% in the O-mode) at low energies (≲ 4 keV; Taverna et al. 2022). Since the magnetic field in the outer layers of a magnetar is expected to locally deviate from a dipole, the surface thermal map is likely different from the usual (dipolar) one, in which the hotter regions are around the magnetic poles, and may change in time (see Tiengo et al. 2013; Borghese et al. 2021, for some ob-

servational evidences; see also De Grandis et al. 2020, 2021 for theoretical considerations). Such a configuration indeed reproduces quantitatively both the observed XMM-Newton 1–10 keV spectrum and the 2–8 keV pulse profile, as well as being compatible with the IXPE detection/upper limits of PD in different energy bins (see Figure 3).

The low pulsed fraction of SGR 1806–20 points to a sizable emitting surface area, as further supported by the inferred BB radius, $\approx 2\,\mathrm{km}$, rather large compared to that usually seen in other magnetar sources ($R_{\mathrm{BB}} \approx 0.1$–$1\,\mathrm{km}$; Olausen & Kaspi 2014, see references therein). The actual size of the emitting region depends on the emission properties of the surface (and also on the geometry and viewing angle of the source). For poorly radiating surfaces, like a magnetic condensate, it is typically larger than R_{BB}. In the model outlined above, the (total) size is $\approx 3.5\,\mathrm{km}$, for an assumed star radius $R_{\mathrm{NS}} = 13\,\mathrm{km}$. The size of the emitting region is not per se a primary factor in establishing the intrinsic polarization properties of the source, which are mostly determined by the physical processes occurring in the surface/magnetosphere and by the source geometry. Indeed, by replacing in our model the magnetic condensate with a fully ionized, magnetized, H atmosphere produces too a large polarization degree at lower energies. On the other hand, the extent to which QED affects the observed polarization depends on the size of the emitting area. If radiation comes from a limited region, across which the direction of the B-field changes little, vacuum birefringence produces almost no detectable effect, i.e. the predicted polarization at infinity is the same with or without QED. In case the emitting area has size $\approx R_{\mathrm{NS}}$, instead, the polarization computed without QED effects is quite lower than that with QED. Despite SGR 1806–20 appears promising in this respect, the low counting statistics prevented us to test the QED vs. no-QED scenario.

The quite large upper limit above $\approx 5\,\mathrm{keV}$ does not rule out different emission scenarios in which the PD is actually larger than $\sim 30\%$, the value predicted by saturated RCS. Phase-averaged values as high as $\sim 55\%$, for instance, may hint at the presence of hot gaseous caps on the star surface, as proposed by Zane et al. (2023) for 1RXS J1708. This possibility would be still consistent with the spectral properties of the source, given that a BB+BB model also provides a good representation of XMM-Newton spectra.

IXPE observations of magnetars have clearly demonstrated the capabilities of polarization measurements in probing the physical conditions in strongly magnetized neutron stars. This includes the presence of QED effects, in favor of which indirect evidences were already gathered from the analysis of 4U 0142+61 and 1RXS J1708. The emerging picture shows substantial differences in the polarization pattern between 4U 0142+61 (and possibly SGR 1806–20) and 1RXS J1708, signalling that emission at higher energies (~ 4–$8\,\mathrm{keV}$) may arise from different physical conditions in the different sources. As the case of SGR 1806–20 shows, collecting enough counts is crucial in providing clear-cut results. Further progress will require observing a larger sample of weaker sources which will be possible for IXPE only with longer exposure times.

Facilities: IXPE, XMM-Newton

<div align="center">REFERENCES</div>

Arnaud, K. A. 1996, in Astronomical Society of the Pacific Conference Series, Vol. 101, Astronomical Data Analysis Software and Systems V, ed. G. H. Jacoby & J. Barnes, 17

Atteia, J. L., Boer, M., Hurley, K., et al. 1987, ApJL, 320, L105, doi: 10.1086/184984

Bachetti, M., Pilia, M., Huppenkothen, D., et al. 2021, ApJ, 909, 33, doi: 10.3847/1538-4357/abda4a

Bachetti, M., Maccarone, T. J., Brightman, M., et al. 2020, ApJ, 891, 44, doi: 10.3847/1538-4357/ab6d00

Baldini, L., Bucciantini, N., Di Lalla, N., et al. 2022, SoftwareX, 19, 101194, doi: 10.1016/j.softx.2022.101194

Bibby, J. L., Crowther, P. A., Furness, J. P., & Clark, J. S. 2008, MNRAS, 386, L23, doi: 10.1111/j.1745-3933.2008.00453.x

Borghese, A., Rea, N., Turolla, R., et al. 2021, MNRAS, 504, 5244, doi: 10.1093/mnras/stab1236

Brivio, R., Ferro, M., Palmer, D. M., et al. 2023, GRB Coordinates Network, 33451, 1

Buccheri, R., Bennett, K., Bignami, G. F., et al. 1983, A&A, 128, 245

Caiazzo, I., González-Caniulef, D., Heyl, J., & Fernández, R. 2022, MNRAS, 514, 5024, doi: 10.1093/mnras/stac1571

De Grandis, D., Taverna, R., Turolla, R., et al. 2021, ApJ, 914, 118, doi: 10.3847/1538-4357/abfdac

De Grandis, D., Turolla, R., Wood, T. S., et al. 2020, ApJ, 903, 40, doi: 10.3847/1538-4357/abb6f9

Di Marco, A., Costa, E., Muleri, F., et al. 2022, AJ, 163, 170, doi: 10.3847/1538-3881/ac51c9

Di Marco, A., Soffitta, P., Costa, E., et al. 2023, AJ, 165, 143, doi: 10.3847/1538-3881/acba0f

Doroshenko, V., Poutanen, J., Tsygankov, S. S., et al. 2022, Nature Astronomy, 6, 1433, doi: 10.1038/s41550-022-01799-5

Duncan, R. C., & Thompson, C. 1992, ApJL, 392, L9, doi: 10.1086/186413

Fernández, R., & Davis, S. W. 2011, ApJ, 730, 131, doi: 10.1088/0004-637X/730/2/131

Fernández, R., & Thompson, C. 2007, ApJ, 660, 615, doi: 10.1086/511810

González-Caniulef, D., Caiazzo, I., & Heyl, J. 2023, MNRAS, 519, 5902, doi: 10.1093/mnras/stad033

González-Caniulef, D., Zane, S., Turolla, R., & Wu, K. 2019, MNRAS, 483, 599, doi: 10.1093/mnras/sty3159

Heyl, J. S., & Shaviv, N. J. 2000, MNRAS, 311, 555, doi: 10.1046/j.1365-8711.2000.03076.x

—. 2002, PhRvD, 66, 023002, doi: 10.1103/PhysRevD.66.023002

Hurley, K., Boggs, S. E., Smith, D. M., et al. 2005, Nature, 434, 1098, doi: 10.1038/nature03519

Kaspi, V. M., & Beloborodov, A. M. 2017, ARA&A, 55, 261, doi: 10.1146/annurev-astro-081915-023329

Kouveliotou, C., Norris, J. P., Cline, T. L., et al. 1987, ApJL, 322, L21, doi: 10.1086/185029

Lai, D. 2023, Proceedings of the National Academy of Science, 120, e2216534120, doi: 10.1073/pnas.2216534120

Laros, J. G., Fenimore, E. E., Klebesadel, R. W., et al. 1987, ApJL, 320, L111, doi: 10.1086/184985

Mazets, E. P., Golenetskii, S. V., Ilinskii, V. N., et al. 1981, Ap&SS, 80, 3, doi: 10.1007/BF00649140

Mereghetti, S., Gotz, D., Ferrigno, C., et al. 2023, GRB Coordinates Network, 33494, 1

Mereghetti, S., Götz, D., Mirabel, I. F., & Hurley, K. 2005a, A&A, 433, L9, doi: 10.1051/0004-6361:200500088

Mereghetti, S., Tiengo, A., Esposito, P., et al. 2005b, ApJ, 628, 938, doi: 10.1086/430943

Nobili, L., Turolla, R., & Zane, S. 2008, MNRAS, 386, 1527, doi: 10.1111/j.1365-2966.2008.13125.x

Olausen, S. A., & Kaspi, V. M. 2014, ApJS, 212, 6, doi: 10.1088/0067-0049/212/1/6

Palmer, D. M., Barthelmy, S., Gehrels, N., et al. 2005, Nature, 434, 1107, doi: 10.1038/nature03525

Santangelo, A., Zane, S., Feng, H., et al. 2019, Science China Physics, Mechanics, and Astronomy, 62, 29505, doi: 10.1007/s11433-018-9234-3

Strohmayer, T. E. 2017, ApJ, 838, 72, doi: 10.3847/1538-4357/aa643d

Strüder, L., Briel, U., Dennerl, K., et al. 2001, A&A, 365, L18, doi: 10.1051/0004-6361:20000066

Taverna, R., Muleri, F., Turolla, R., et al. 2014, MNRAS, 438, 1686, doi: 10.1093/mnras/stt2310

Taverna, R., Turolla, R., Gonzalez Caniulef, D., et al. 2015, MNRAS, 454, 3254, doi: 10.1093/mnras/stv2168

Taverna, R., Turolla, R., Suleimanov, V., Potekhin, A. Y., & Zane, S. 2020, MNRAS, 492, 5057, doi: 10.1093/mnras/staa204

Taverna, R., Turolla, R., Muleri, F., et al. 2022, Science, 378, 646, doi: 10.1126/science.add0080

Thompson, C., & Duncan, R. C. 1993, ApJ, 408, 194, doi: 10.1086/172580

Thompson, C., Lyutikov, M., & Kulkarni, S. R. 2002, ApJ, 574, 332, doi: 10.1086/340586

Tiengo, A., Esposito, P., Mereghetti, S., et al. 2013, Nature, 500, 312, doi: 10.1038/nature12386

Turner, M. J. L., Abbey, A., Arnaud, M., et al. 2001, A&A, 365, L27, doi: 10.1051/0004-6361:20000087

Turolla, R., Zane, S., & Watts, A. L. 2015, Reports on Progress in Physics, 78, 116901, doi: 10.1088/0034-4885/78/11/116901

van Adelsberg, M., & Perna, R. 2009, MNRAS, 399, 1523, doi: 10.1111/j.1365-2966.2009.15374.x

Vaughan, B. A., van der Klis, M., Wood, K. S., et al. 1994, ApJ, 435, 362, doi: 10.1086/174818

Weisskopf, M. C., Guainazzi, M., Jahoda, K., et al. 2010, ApJ, 713, 912, doi: 10.1088/0004-637X/713/2/912

Weisskopf, M. C., Soffitta, P., Baldini, L., et al. 2022, Journal of Astronomical Telescopes, Instruments, and Systems, 8, 1 , doi: 10.1117/1.JATIS.8.2.026002

Woods, P. M., Kouveliotou, C., Finger, M. H., et al. 2007, ApJ, 654, 470, doi: 10.1086/507459

Younes, G., Baring, M. G., Kouveliotou, C., et al. 2017, ApJ, 851, 17, doi: 10.3847/1538-4357/aa96fd

Younes, G., Kouveliotou, C., & Kaspi, V. M. 2015, ApJ, 809, 165, doi: 10.1088/0004-637X/809/2/165

Zane, S., Taverna, R., González-Caniulef, D., et al. 2023, ApJL, 944, L27, doi: 10.3847/2041-8213/acb703